Three-pass 3-d migration on a hexagonal grid

Marta Jo Woodward

ABSTRACT

Two-pass 15-degree migration on a square grid is compared to three-pass 15-degree migration on a hexagonal grid. The latter is found to be more accurate, more symmetrical and more efficient than the former.

INTRODUCTION

Two papers appeared in SEP-38 comparing the advantages and disadvantages of 3-d seismic data collection and *one-pass* migration on hexagonal and square grids (Woodward and Muir, 1984a; Woodward and Muir, 1984b). They showed that hexagonal grids sample regions circularly bandlimited in k_x and k_y 13.4% more efficiently than square grids—allowing in-line midpoint spacings $\frac{2}{\sqrt{3}}$ times longer than their square counterparts. They also demonstrated that hexagonal grids permit representations of the 2-d Laplacian (∇^2) used in explicit 3-d migration that are marginally both more accurate and more symmetrical than those corresponding to square grids. Unfortunately, it was also found that the computational effort required to perform explicit 3-d migration on a hexagonal grid is approximately 40% greater than on a square grid, due to hexagonal Laplacians being larger than square Laplacians of comparable accuracy, and due to their related requirement for smaller depth-steps (Woodward, 1984d).

Jakubowicz and Levin (1983) introduced a *two-pass* alternative to one-pass migration on a square grid by showing that sequential migration in two orthogonal directions is equivalent to full 3-d wave equation migration in a homogeneous medium of velocity v:

$$\begin{aligned} k_{z_1}^2 &= \omega^2 - v^2 {k_x}^2 \\ k_{z_2}^2 &= k_{z_1}^2 - v^2 {k_y}^2 \\ &= \omega^2 - v^2 {k_x}^2 - v^2 {k_y}^2. \end{aligned} \tag{1}$$

Using a generalized form of the Pythagorean theorem, Woodward and Muir (1984b; 1984c) extended this proof to *three-pass* migration—showing that sequential under-migration with a velocity

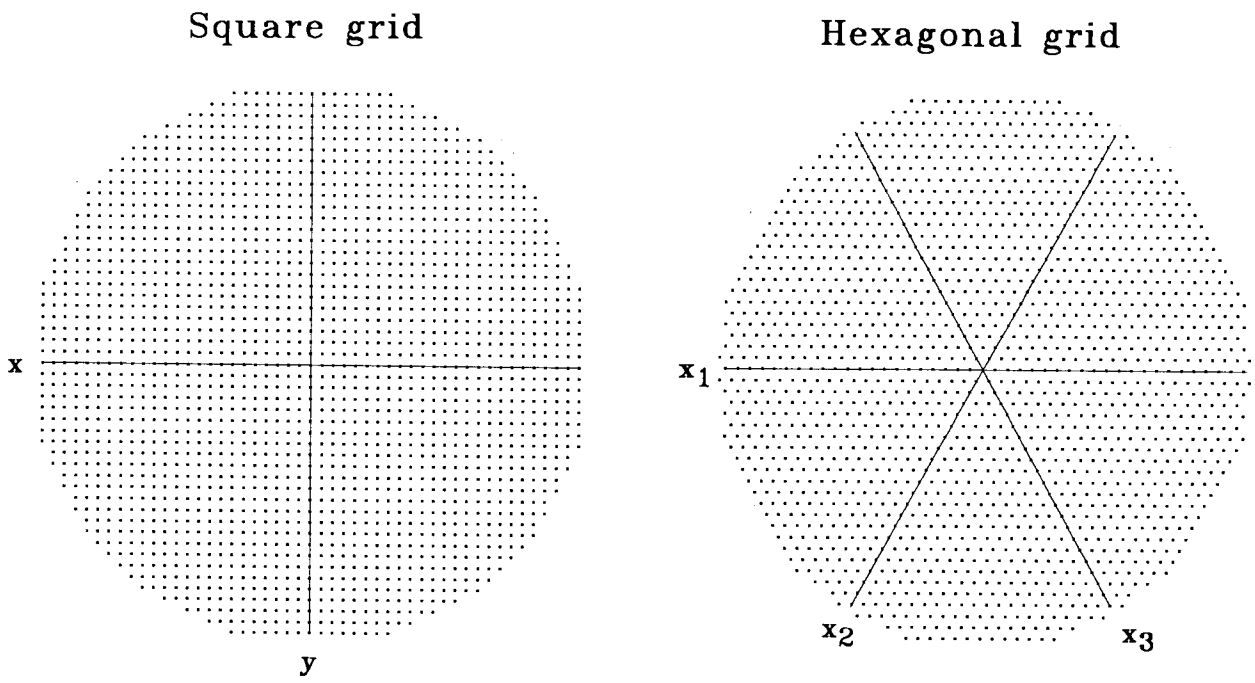

FIG. 1. Square and hexagonal midpoint grids with comparable aliasing characteristics in the spatial frequency domain. Line spacings for the two patterns are equivalent; in-line midpoint intervals are 16% longer on the right than on the left.

$\sqrt{\frac{2}{3}}v$ in three directions on a hexagonal grid is also equivalent to full 3-d wave equation migration in a homogeneous medium of velocity v:

$$\begin{aligned} k_{r_1}^2 &= \omega^2 - \tfrac{2}{3}v^2 k_{x_1}^2 \\ k_{r_2}^2 &= k_{r_1}^2 - \tfrac{2}{3}v^2 k_{x_2}^2 \\ k_{r_3}^2 &= k_{r_2}^2 - \tfrac{2}{3}v^2 k_{x_3}^2 \\ &= \omega^2 - \tfrac{2}{3}v^2 \left(k_{x_1}^2 + k_{x_2}^2 + k_{x_3}^2\right). \end{aligned} \tag{2}$$

For the purpose of clarifying equations (1) and (2), this paper first provides examples of two and three-pass Stolt migration worked on square and hexagonal grids. It then examines 15-degree equivalents to equations (1) and (2), and evaluates two and three-pass 15-degree migrations as approximations to full 3-d migration. Three-pass 15-degree migration is shown to be both more accurate and more symmetrical than its two-pass counterpart. Finally, the computational costs of two and three-pass 15-degree schemes are compared, and the latter is found to be more efficient than the former.

THREE-PASS STOLT MIGRATION

Figure 1 shows square and hexagonal midpoint grids with comparable aliasing characteristics

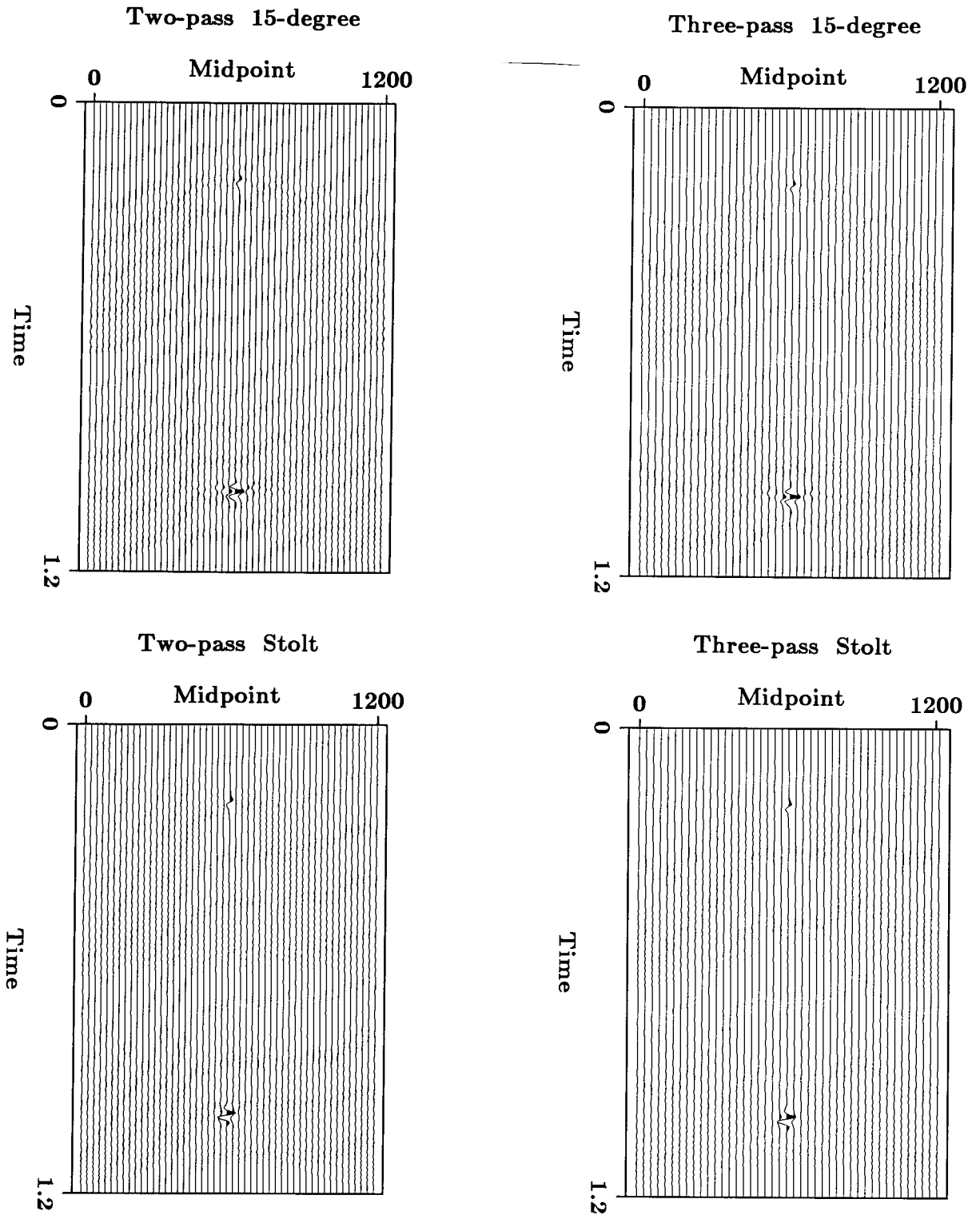

FIG. 2. Two and three-pass 15-degree migrations and two and three-pass Stolt migrations of a synthetic data set consisting of two zero-phase, constant-velocity hyperboloids sampled according to Figure 1. The trace spacings on the three-pass sections are 16% larger than on the two-pass sections, reflecting the different midpoint spacings of their respective hexagonal and square migration grids. The clip values have been adjusted to equalize the maximum kicks on all the plots.

in the spatial frequency domain, designed for the collection of 3-d seismic data over a circular region. Line spacings for the two patterns are equivalent; in-line midpoint intervals are $\frac{2}{\sqrt{3}}$ longer on the right than on the left. Two-pass migration on the square grid corresponds to fully migrating (with a velocity v) the 49 lines parallel to the x-axis, then resorting and fully migrating the 49 lines parallel to the y-axis. Three-pass migration on the hexagonal grid corresponds to under-migrating (with a velocity $\sqrt{\frac{2}{3}}v$) the 49 lines parallel to the x_1 axis, resorting and under-migrating the 49 lines parallel to the x_2 axis, and then, finally, resorting and under-migrating the 49 lines parallel to the x_3 axis. The results of two-pass and three-pass Stolt migration of a synthetic data set consisting of two zero-phase, constant-velocity hyperboloids sampled according to Figure 1 are shown in the lower half of Figure 2. Both display the 90-degree phase-shift expected for 3-d migration. While they are visually and theoretically indistinguishable, it should be noted that the hexagonal example required 50% more computational effort than the square example.

THREE PASS 15-DEGREE MIGRATION

Accuracy and symmetry: observations

Equations (1) and (2) strictly hold only for homogeneous media and complete, 90-degree schemes such as the Stolt migrations of the preceding section. However, it has been shown that they may also be applied with reasonable success to inhomogeneous media—where approximate finite-difference schemes must be used (Gibson et al., 1983). 15-degree approximation equivalents to equations (1) and (2) are given in the Appendix. Comparison of these approximations with full accuracy 3-d equations permits calculation of relative phase errors for two-pass and three-pass 15-degree migration. These errors are shown for 15°, 45° and 60° dips in Figure 3. They are plotted as functions of grid azimuth—the angle measured between the first-pass (x or x_1) axis and the dip direction; the dashed lines correspond to two-pass migration, the solid lines to three-pass. Examination of the graphs yields three conclusions. First, two and three-pass 15-degree migration schemes both undermigrate 3-d seismic data—just as one-pass 15-degree migration undermigrates 2-d data. Second, three-pass is more symmetrical than two-pass migration, manifesting a smaller variation in phase error over a longer repeat interval (180° as opposed to 45°). Third, three-pass 15-degree migration is almost always more accurate than its two-pass counterpart.

These differences may be explained by recognizing that two-pass and three-pass migration differ in the *apparent* dips they present to the 15-degree operator. Since the 15-degree approximation to the scalar wave equation decreases in accuracy for high dips (especially for dips steeper than 30°), the scheme presenting the lowest apparent dips is most accurate. Three-pass migration is distinguished from two-pass migration in that each migration is a partial (or under) migration with velocity $\sqrt{\frac{2}{3}}v$. Consequently, for a given dip, the sine of the *apparent* dip perceived by

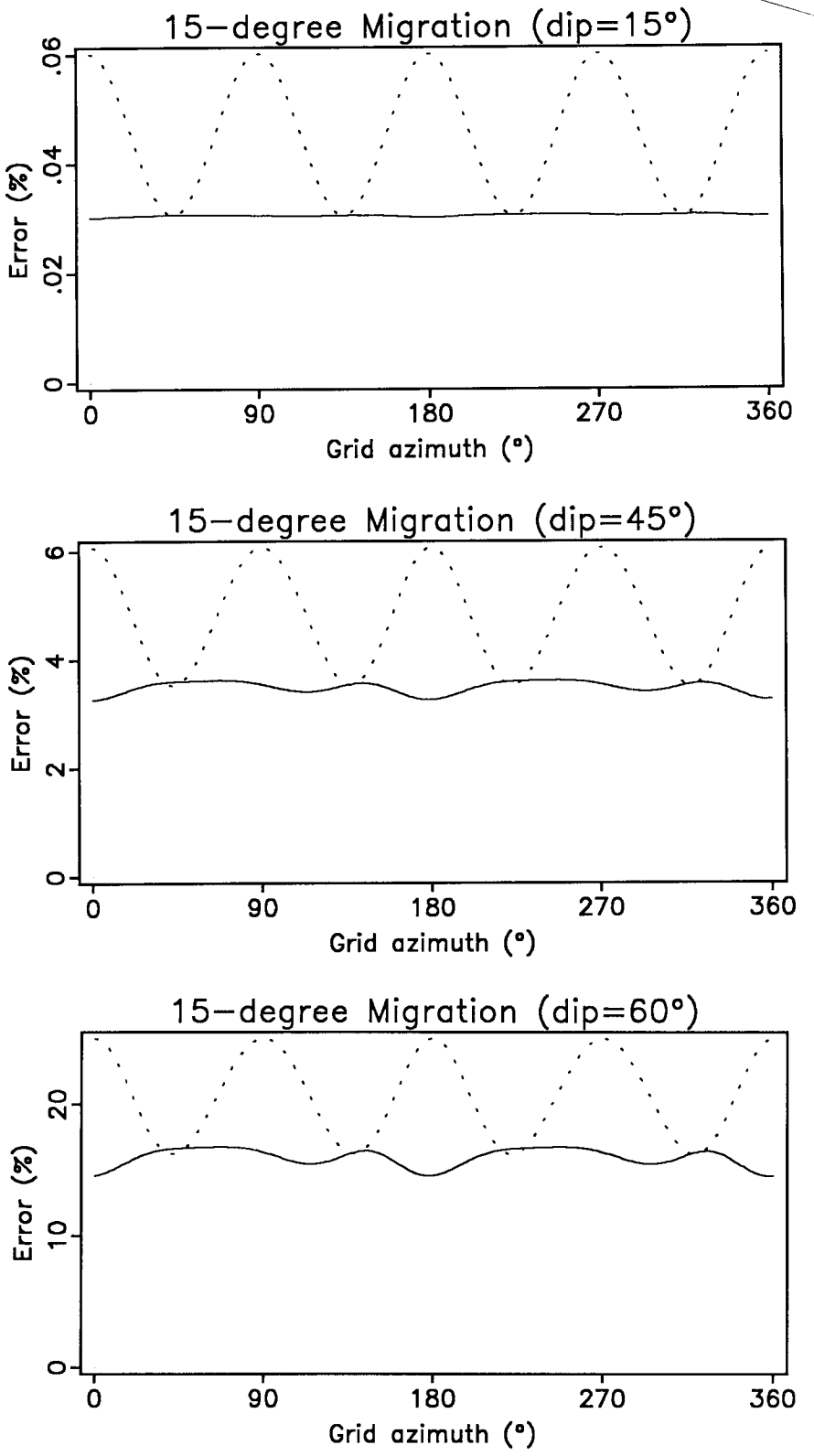

FIG. 3. Percent phase errors for two-pass (dashed line) and three-pass (solid line) 15-degree, 3-d migration—for 15°, 45° and 60° dips. Expressions for the phase errors appear in the Appendix.

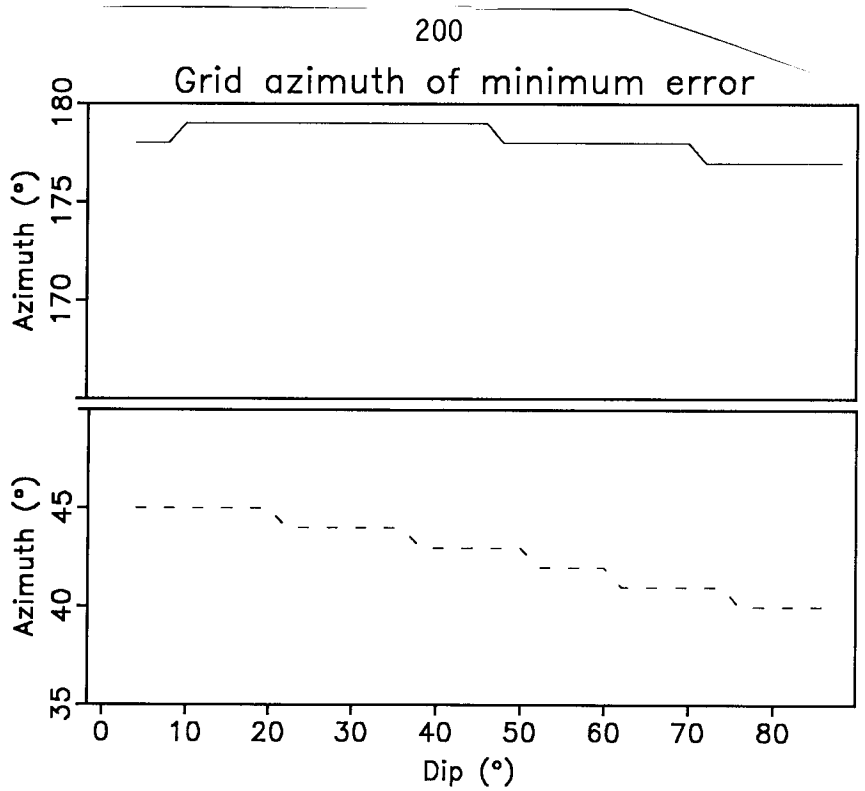

FIG. 4. Grid azimuth corresponding to minimum phase error as a function of dip for two (dashed line) and three-pass (solid line) 15-degree migration.

the 15-degree operator is $\sqrt{\frac{2}{3}}$ (or 18%) smaller for three-pass than for two-pass migration—and the former will usually be more accurate than the latter. (This reasoning is similar to cascaded migration arguments presented by Larner and Beasley, 1986.)

Three-pass migration will occasionally be less accurate than two-pass, because the preceding argument is complicated by the issue of grid orientation. Figure 4 plots the grid azimuth corresponding to minimum phase error as a function of dip for two and three-pass 15-degree migration, dashed and solid lines assigned as above. The maximum apparent dip perceived by two-pass migration goes through a pronounced minimum when its associated square computational grid is oriented at an angle of 45° to the dip direction—when the apparent dip is reduced by a factor of cos(45°) (or 29%). (For steep dips, where first-pass dip-steepening must be taken into account, the minimum is at slightly less than 45°.) Since three-pass hexagonal grids are more symmetrical than two-pass square grids, grid rotation contributes little to three-pass apparent dip reduction; one axis will always be within 30° of the maximum dip direction—corresponding to a dip reduction factor of only cos(30°) (or 13%, for a total of 29%, including the under-migration factor). Consequently, the two-pass method can be marginally more accurate for grid azimuths in the vicinity of 45° or 135°. Figure 4 indicates that apparent dips for three-pass migration are minimized by orienting the x_1-axis parallel to the dip direction; this procedure minimizes dips in the second and third-pass migrations, subsequent to first-pass steepening.

Accuracy and symmetry: examples

While the superiority of three-pass to two-pass migration appears highly significant in Figure 3, its superiority in practical applications is more subtle. Two examples are worked in this paper, comparing two and three-pass migration for both symmetrical and asymmetrical reflectors in homogeneous media. The first, symmetrical example appears in the top panels of Figure 2—where the the results of two and three-pass migration of the hyperboloid synthetics described in the Stolt migration section are exhibited. Although the two results are very similar, the three-pass picture does display more undermigration artifacts—indicative of the fact that it is marginally less successful at handling dips at most azimuths.

The second, asymmetrical example appears in Figures 5a and 5b. Here the synthetic data set consisted of a planar reflector dipping at an angle of 45°. It was sampled over a circular region similar to that shown in Figure 1—but sampled twice as densely. Two-pass and three-pass migrations were performed twice each for several depth-steps $\Delta\tau$: once with the x and x_1 axes oriented parallel to the dip direction (Figure 5a); once with them oriented at 45° to the dip direction (Figure 5b). (In both instances, the dipping reflector intersected the surface at the edge of the circular sampling region.) Judgement of the panels on the steepness, truncation placement and basal sharpness of their images, as well as on their overall level of artifacts, yields three conclusions. First, as predicted by Figure 3, the superior symmetry of three-pass migration is readily apparent: for equivalent $\Delta\tau$'s, the qualities of the three-pass 0° and 45°-azimuth panels are more nearly identical than those of the same two-pass panels. Second, also as predicted by Figure 3, three-pass migration is clearly more accurate than two-pass migration for 0°-azimuths: the three-pass panels are superior to the two-pass panels not only for equivalent $\Delta\tau$'s, but also for $\Delta\tau$ ratios of 2:1. Third, for the 45°-azimuth panels, where Figure 3 predicts the marginal superiority of two-pass migration, the three-pass panels are still slightly better—as judged mainly on the criteria of sharpness and artifact level. This result is discussed in the following section, where the contrasting sensitivities of the two migration schemes to the depth-step parameter $\Delta\tau$ are explored.

Efficiency: observations

The amount of computational work required for multiple-pass 15-degree time migration is equal to $np \cdot nx \cdot n\tau$—the number of passes times the number of traces in each pass times the number of depth steps in each pass. Given that hexagonal, three-pass sampling grids need only $\frac{\sqrt{3}}{2}$ as many traces as their square, two-pass counterparts, the ratio of work required for two-pass and three-pass migrations becomes:

$$\frac{W_s}{W_h} = \frac{2}{3} \cdot \frac{2}{\sqrt{3}} \cdot \frac{n\tau_s}{n\tau_h} = \frac{4}{3\sqrt{3}} \cdot \frac{n\tau_s}{n\tau_h}, \tag{3}$$

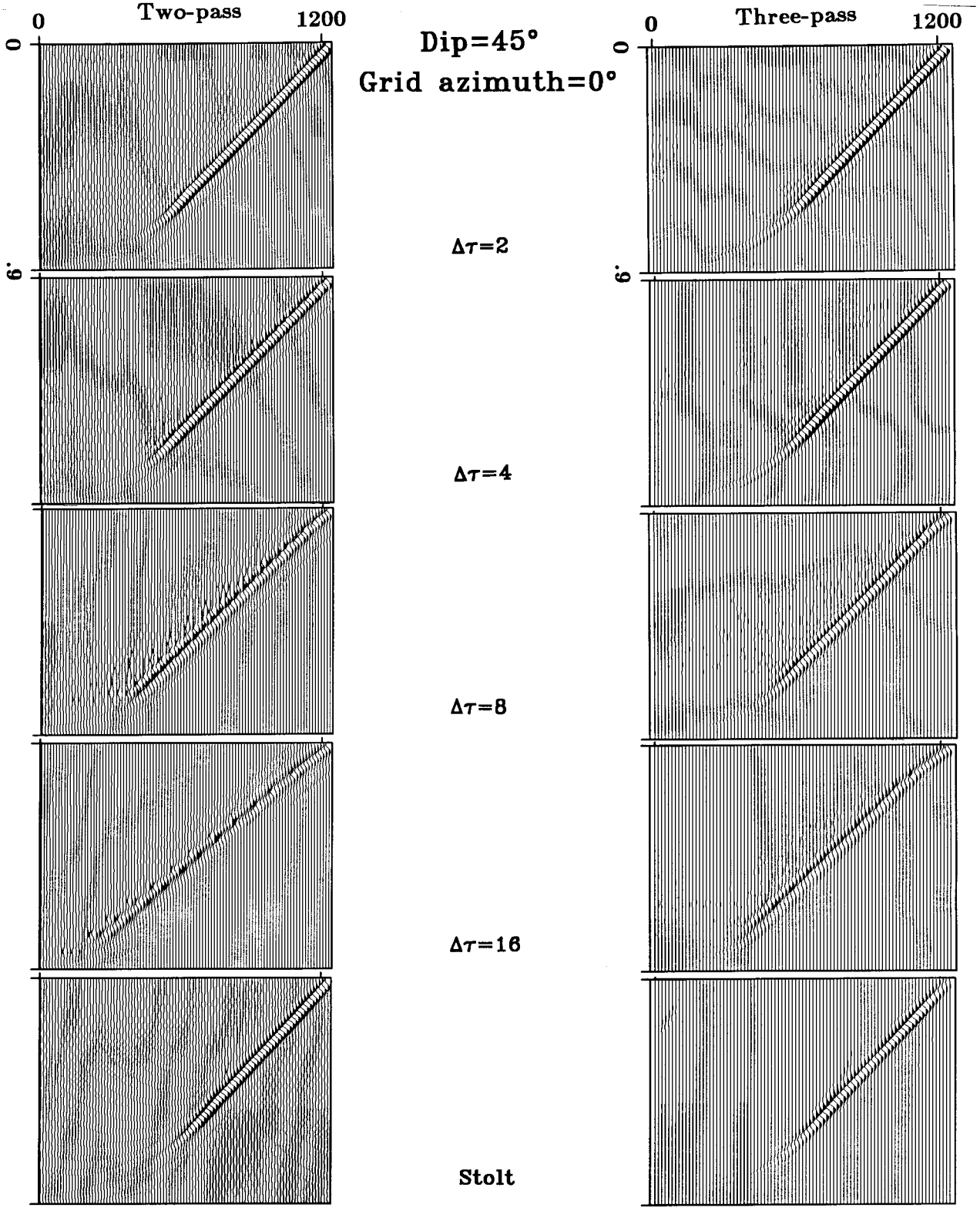

FIG. 5a. This figure compares two and three-pass 15-degree migrations of a planar reflector dipping at 45° in the direction of the first-pass (x or x_1) axis, and sampled over a circular region similar to that in Figure 1 (but sampled twice as densely). Migrations were performed for $\Delta\tau$ equal to 2, 4, 8 and 16 times the 4 ms time interval. Full accuracy Stolt migrations are shown for comparison at the bottom. Trace spacings on the three-pass sections are 16% larger than on the two-pass sections, reflecting the different midpoint spacings of hexagonal and square grids. The sections were lowpass filtered at 20 Hz; clip values were adjusted to equalize maximum kicks.

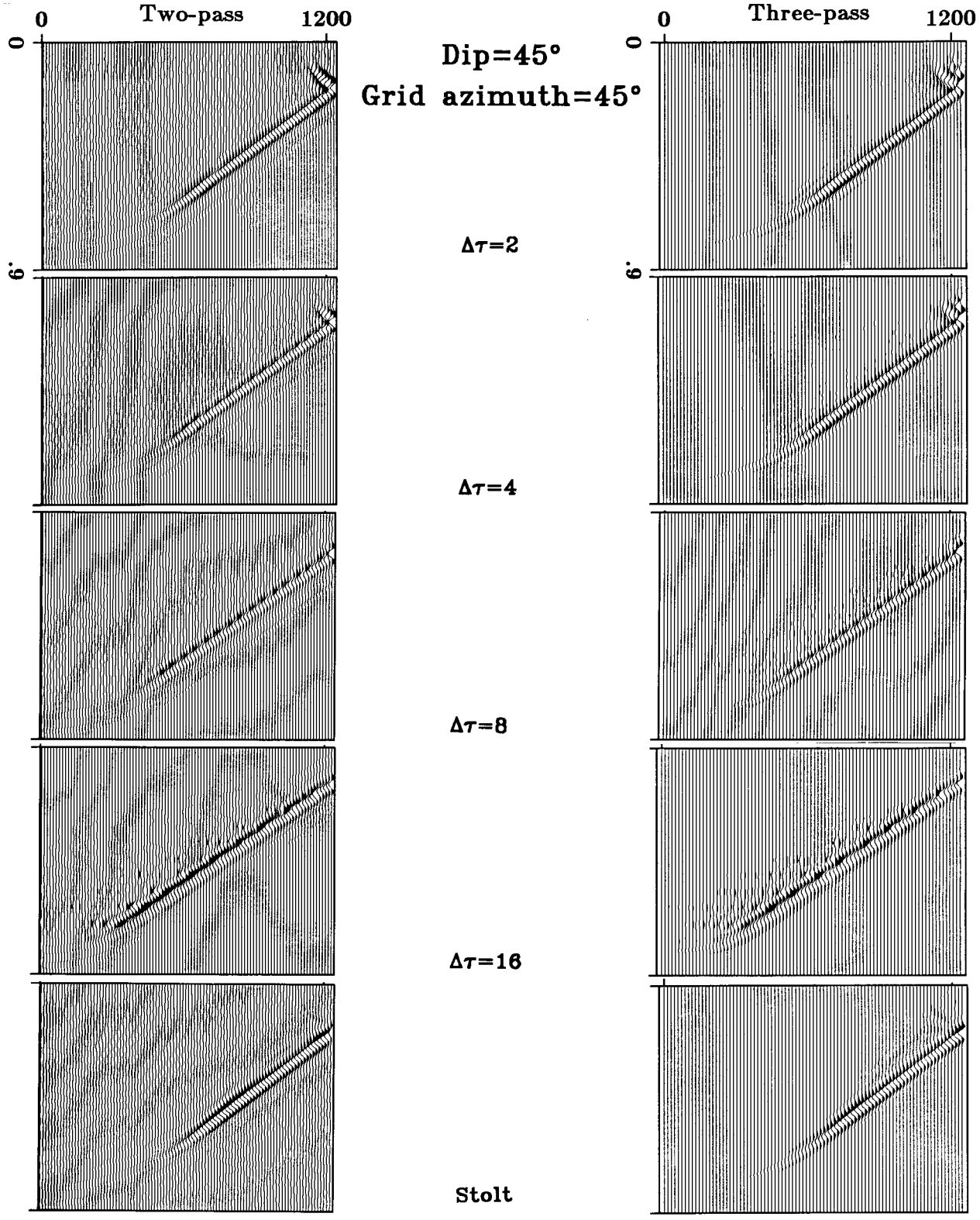

FIG. 5b. This figure compares two and three-pass 15-degree migrations of a planar reflector dipping at 45°, striking 45° with respect to the first-pass (x or x_1) axis, and sampled over a circular region similar to that in Figure 1 (but sampled twice as densely). Migrations were performed for $\Delta\tau$ equal to 2, 4, 8 and 16 times the 4 ms time interval. Full accuracy Stolt migrations are shown for comparison at the bottom. Trace spacings on the three-pass sections are 16% larger than on the two-pass sections, reflecting the different midpoint spacings of hexagonal and square grids. The sections were lowpass filtered at 20 Hz; clip values were adjusted to equalize maximum kicks.

where $n\tau_s$ and $n\tau_h$ refer to the number of depth-steps required for square and hexagonal schemes, respectively.

In their paper on cascaded migration, Larner and Beasley (op. cit.) note that the basic equation used in 15-degree time migration is

$$\delta_t \delta_\tau P = \left(\frac{v^2 \Delta\tau \Delta t}{16 \Delta x^2} \right) \delta_{xx} P, \tag{4}$$

where v is the velocity used in the migration, Δt is the time sampling interval, Δx is the trace spacing, $\Delta\tau$ is the depth-step, δ_{xx} is the second difference operator in the x-direction, δ_t and δ_τ are the first difference operators in the t and τ directions, and $P(x, \tau, t)$ is the wavefield. They then observe that, for a given data set, the value of the parenthesized coefficient in this equation determines the accuracy of the migration—thereby justifying the combination of large depth-steps with small velocities in cascaded migration schemes. A similar argument can be used to justify the use of larger (fewer) depth-steps in three-pass migration than in two-pass migration. Since the migration velocity used in the former is $\sqrt{\frac{2}{3}}$ times that used in the latter, and since trace spacings are $\frac{\sqrt{3}}{2}$ times as large,

$$\frac{n\tau_s}{n\tau_h} = \frac{\Delta\tau_h}{\Delta\tau_s} = \frac{v_s^2 \Delta x_h^2}{v_h^2 \Delta x_s^2} = 2; \tag{5}$$

for a given data set, three-pass migration may achieve finite-difference accuracy equivalent to that of two-pass migration with half as many depth-steps. Combination of this result with equation (3) leads to the conclusion that

$$\frac{W_s}{W_h} = 1.54; \tag{6}$$

hexagonal three-pass migration requires only 65% as much computational effort as two-pass migration. (If the sampling efficiency of the hexagonal grid is neglected, three-pass migration can be shown to be 30% more work than two-pass.)

Efficiency: examples

These conclusions are substantiated by Figures 5a and 5b, although the examples are complicated by the phase-error contrasts. Where the phase error of three-pass migration is smaller than that of two-pass migration (i.e., Figure 5a), three-pass migration remains superior to two-pass migration for $\Delta\tau$ ratios of 2:1. Where the phase error of three-pass migration is comparable or larger than that of two-pass migration (i.e., Figure 5b), three-pass migration is superior to two-pass migration for $\Delta\tau$ ratios of 1:1, and only marginally inferior for ratios of 2:1.

CONCLUSION

Given cascaded migration—where 15-degree finite-difference migration achieves high accuracy for steep dips at low cost through a series of large depth-step residual migrations—the superior

symmetry and accuracy characteristics of three-pass 3-d migration become insignificant; with the cascade method two-pass 3-d migrations may always be made as accurate and symmetric as their three-pass equivalents (Larner and Beasley, op. cit.). Nevertheless, 3-d cascaded migration implemented on a hexagonal grid will always be more efficient than cascaded migration implemented on a square grid; because of the larger midpoint spacings and lower $(\sqrt{\frac{2}{3}})$ migration velocity, three-pass schemes can achieve superior results for the same computational effort.

ACKNOWLEDGEMENTS

Thanks go to Francis Muir for pointing out and coding up equation (A2).

REFERENCES

Gibson, B., Larner, K., and Levin, S., 1983, Efficient 3-d migration in two steps, Geophysical Prospecting, 31, p. 1-33.

Jakubowicz, H., and Levin, S., 1983, A simple exact method of 3-d migration—theory, Geophysical Prospecting, 31, p. 34-56.

Larner, K., and Beasley, C., 1986, Cascaded migrations: a way of improving the accuracy of finite-difference migration, in press.

Woodward, M., and Muir, F., 1984a, Hexagonal sampling, SEP-38.

Woodward, M., and Muir, F., 1984b, Hexagonal finite difference operators and 3-d wave equation migration, SEP-38.

Woodward, M., and Muir, F., 1984c, Hexagonal sampling and hexagonal finite difference operators, talk presented at Fallen Leaf Lake.

Woodward, M., 1984d, Acquisition and migration of three-dimensional seismic surveys, undistributed orals paper.

APPENDIX

The 15-degree approximation equivalents to equations (1) and (2) are

$$\frac{{}_{15}k_{\tau_1}^2}{\omega} = 1 - \frac{v^2 {k_x}^2}{2\omega^2}$$

$$\frac{{}_{15}k_{\tau_2}^2}{\omega} = 1 - \frac{v^2 {k_x}^2}{2\omega^2} - \frac{v^2 k_y^2}{2\omega^2\left(1 - \frac{v^2 k_x^2}{2\omega^2}\right)}$$

$$= 1 - \frac{\rho^2 \cos^2(\theta)}{2} - \frac{\rho^2 \cos^2(\theta + 90°)}{2\left(1 - \frac{\rho^2 \cos^2(\theta)}{2}\right)}, \qquad \text{(A1)}$$

(Jakubowicz and Levin, op. cit.), and

$$\frac{{}_{15}k_{\tau_1}^2}{\omega} = 1 - \frac{v^2 {k_1}^2}{3\omega^2}$$

$$\frac{{}_{15}k_{\tau_2}^2}{\omega} = 1 - \frac{v^2 {k_1}^2}{3\omega^2} - \frac{v^2 k_2^2}{3\omega^2\left(1 - \frac{v^2 k_1^2}{3\omega^2}\right)}$$

$$\frac{{}_{15}k_{\tau_3}^2}{\omega} = 1 - \frac{v^2 {k_1}^2}{3\omega^2} - \frac{v^2 k_2^2}{3\omega^2\left(1 - \frac{v^2 k_1^2}{3\omega^2}\right)} - \frac{v^2 k_3^2}{3\omega^2\left(1 - \frac{v^2 k_1^2}{3\omega^2} - \frac{v^2 k_2^2}{3\omega^2\left(1 - \frac{v^2 k_1^2}{3\omega^2}\right)}\right)}$$

$$= 1 - \frac{\rho^2 \cos^2(\theta)}{2} - \frac{\rho^2 \cos^2(\theta + 60°)}{2\left(1 - \frac{\rho^2 \cos^2(\theta)}{2}\right)} - \frac{\rho^2 \cos^2(\theta + 120°)}{2\left(1 - \frac{\rho^2 \cos^2(\theta)}{2} - \frac{\rho^2 \cos^2(\theta + 60°)}{2\left(1 - \frac{\rho^2 \cos^2(\theta)}{2}\right)}\right)}, \quad \text{(A2)}$$

respectively. For both equations: θ is the grid azimuth—the angle measured between the first-pass (x or x_1) axis and the dip direction; ρ^2 is the squared cosine of the dip—

$$\rho^2 = \frac{v^2}{\omega^2}\left(k_x^2 + k_y^2\right) = \frac{2v^2}{3\omega^2}\left(k_1^2 + k_2^2 + k_3^2\right). \quad \text{(A3)}$$

Comparison of equation (1) with equation (A1), and equation (2) with equation (A2), permits calculation of the relative phase errors for two-pass and three-pass 15-degree migration—$\left({}_{15}k_{\tau_2} - k_{\tau_2}\right)/k_{\tau_2}$ and $\left({}_{15}k_{\tau_3} - k_{\tau_3}\right)/k_{\tau_3}$, respectively. They are plotted in Figure 3.